

Controlled Wireless Channel using Multi-Antenna Multi-IRS Assisted Communication System: A Comprehensive Performance Analysis

Suresh Penchala , Shравan Kumar Bandari , *Member, IEEE*, Vakamulla Mani , *Senior Member, IEEE*, and Anastasios Drosopoulos , *Member, IEEE*

Abstract—To address societal demands, upcoming communication systems must manage multiple tasks simultaneously, thereby increasing circuit complexity and error rates. These challenges can be mitigated with intelligent reflecting surface (IRS) by utilizing cost-effective reconfigurable metamaterials to manipulate wireless propagation channels. The study investigates the performance analysis of a multi-antenna multi-IRS-assisted communication system in a generalized $\eta - \mu$ fading channel assuming non-line-of-sight (NLOS) scenario between the base station (BS) and the user equipment (UE) using the moment-generating function (MGF) approach. The theoretical expressions for the bit error rate (BER), and Ergodic capacity (EC) are derived for the system model under consideration. Energy efficiency (EE) was also evaluated for completeness. A mean Monte-Carlo (MC) transceiver simulation test bed is provided to validate the obtained theoretical expressions. The derived theoretical formulae cover Nakagami- m , Nakagami- q , and Rayleigh channels as corner cases to cover the practical indoor and outdoor scenarios. Improved performance is observed with more antennas at the BS and UE, more IRSs, more reflecting elements, IRS placement near BS or UE, high μ , and low η values. It was noticed that the triple-IRS system offers better BER, enhanced EC, more energy efficient than the single-IRS system, and achieves 8 dB gain at BER point of 10^{-5} , 2.82 (b/s/Hz) improvement in EC, and 3.5 times energy efficient at average achievable rate 25 (b/s/Hz). Moreover, employing multiple antennas achieves 6 dB improvement at BER value of 10^{-5} , enhanced achievable rate, and in turn improves energy efficiency. Lastly, placing the IRS either near BS or UE is more beneficial than setting it at mid-way where the BER reduces from 10^{-2} to 10^{-9} , EC of 2 (b/s/Hz) gain, and can design a 3 times better energy efficient system.

Link to graphical and video abstracts, and to code:
<https://latam.ieceer9.org/index.php/transactions/article/view/9318>

Index Terms—BER, EC, EE, multi-IRS multi-antenna, $\eta - \mu$ fading channel.

The associate editor coordinating the review of this manuscript and approving it for publication was Carolina Del-Valle-Soto (*Corresponding author: Suresh Penchala*).

Suresh Penchala, and S. K. Bandari are with the Department of Electronics and Communication Engineering, National Institute of Technology Meghalaya, India (e-mails: penchalesuresh@gmail.com, and shravnbandari@nitm.ac.in).

V. Mani is with the Department of Electronics and Communication Engineering, National Institute of Technology Warangal, India (e-mail: vvmani@nitw.ac.in).

A. Drosopoulos is with the Department of Electrical and Computer Engineering, University of Peloponnese, Greece (e-mail: drosop@uop.gr).

I. INTRODUCTION

EMERGING as a pivotal technology, intelligent reflecting surfaces (IRS) hold great promise in shaping the evolution of forthcoming wireless communication systems (6G) [1], [2]. In a broader sense, IRS belongs to the category of metasurfaces engineered for adaptability, allowing for modifications in the amplitude, phase, and polarization of the reflected electromagnetic (EM) field from the surface [3]. IRS technology is versatile and applicable across diverse scenarios such as indoor and outdoor wireless networks, 6G cellular environments, and satellite communication systems [4]. Its capabilities offer the prospect of enhancing wireless communication efficiency and performance by addressing multipath fading, minimizing interference, and expanding coverage areas [5]. Its primary function resembles that of relay technology, focusing on enhancing propagation environments like extending coverage and addressing blind spots. Nevertheless, unlike relays, which actively process and amplify received signals before re-transmission, IRS operates passively with low cost reflecting elements, solely reflecting the EM signals [6].

Despite increasing interest in IRS technology, its adoption in practical applications requires substantial time and resources. The investment necessitates that the IRS demonstrate notable performance benefits compared to established technologies [7]. Conventional channel models that only consider large-scale shadowing are not sufficient to accurately represent the complex propagation effects of 5G and 6G wireless networks, given their wide range of use cases and applications [8]. The authors in [9] expanded their investigation on the IRS to include unmanned aerial vehicle (UAV) networks. An optimization problem was formulated with the objective of maximizing the achievable throughput for the proposed UAV system that utilizes IRS technology.

IRS represents an emerging technology that can manage channel impairments by utilizing various reflective surfaces [10]. The study delved into performance evaluation of the IRS-enhanced communication system in outdoor and indoor radio scenarios, considering Rician distributions, and employing the Laguerre series method [11], the system's symbol error probability (SEP) for the IRS-assisted single-input-single-output (SISO) system is demonstrated in Rayleigh fading channels [12]. An analysis is conducted on the symbol error rate (SER) probability of a wireless communication system assisted by the IRS over a Nakagami- m fading channel [13], Weibull [14],

and the BER for the system aided by the IRS is reported in log-normal fading channels [15] fading models, utilizing the moment generating function (MGF) methodology and considering independent and identically distributed (IID) fading distributions in a NLOS case employing single IRS. Furthermore, the significant advantages of the IRS make it a commonly utilized tool in enhancing wireless communications, often through the implementation of multi-IRS systems to enhance the coverage and reliability [16]. Therefore, wireless signals can be efficiently reflected during transmission from the base station (BS) to the user equipment (UE). [17] has proposed several multiple-IRS-assisted 6G wireless networks to meet future demands. Study in [17] suggests that multiple IRSs can substantially enhance wireless communication coverage, capacity, and service quality. When multiple IRSs are utilized cooperatively, the signal power at the UE is significantly boosted [18]. Additionally, placing IRSs in various locations ensures that signals can still reach the UE through alternative paths even if some experience deep fading.

The $\eta-\mu$ distribution is a generalized fading framework that has been extensively used in wireless communication to analyze the performance of any system model under consideration [19]. The parameter η defines the shape of the channel fading distribution, whereas the parameter μ indicates the number of multipath clusters or the fading intensity. It is especially well-suited for describing situations in which both multipath propagation and interference effects occur, such as urban or indoor environments. Due to its flexible fading parameters adjustment, $\eta-\mu$ covers some of the well-known fading distributions such as Rayleigh, Nakagami- m , and Nakagami- q as special cases [19]. Given the aforementioned points, it is clear that generalized wireless statistical information is necessary to cover a wide range of scenarios. Recently, authors in [20] derived the probability density function (PDF) of the envelope of $\eta-\mu$ channel assuming discrete values of the number of in-phase and quadrature components. The characteristic function (CHF) of the proposed analytical expression has been formulated and applied to the single IRS-supported communication system to derive the outage probability (OP) and the bit error probability (BER). However, the mathematical complexity dramatically increases with the number of reflecting elements and cascaded channels.

Building upon the survey mentioned earlier, it is apparent that multiple-IRSs can enhance the overall wireless communication system performance. On the other hand, system analysis under generalized fading channel models covers special scenarios as corner cases. It has been observed that the performance analysis of multi-IRS multi-input-multi-output (MIMO) systems under generalized fading models is still in its infancy. Motivated by the above facts, in this work we consider a multi-IRS supported system model in the NLOS case with all the wireless channel links as $\eta-\mu$ for the MIMO scenario. An in-depth analysis of various performance metrics, such as BER, Ergodic capacity (EC), and energy efficiency (EE) under different parameter settings namely, the number of reflecting elements, number of antennas employed at BS and UE, number of IRSs, location of the IRS, transmit power, and fading parameters are performed. The key contribution of this

study can be succinctly described as follows:

- Due to the sophisticated nature of the complex channel between the BS-IRS links, and the channel between the IRS-user links, we formulated a step-by-step relationship between the input-output system model of the proposed MIMO multiple-IRS communication system. In this formulation, we have also considered the distance-based path loss component to ensure a comprehensive and realistic representation of the channel conditions.
- With the aid of the derived signal-to-noise ratio of the system model under consideration, applying central limit theorem (CLT), we deduced the statistical information of the overall cascaded wireless channel links in terms of the mean and variance.
- Using the MGF approach, we derived the analytical expression of the probability of bit error rate under generalized $\eta-\mu$ fading distribution in terms of the stakeholder parameters such as the number of reflecting elements, number of IRSs, number of antennas at the BS and UE, large-scale path loss, and fading parameters.
- A framework to find the mathematical complexity of deriving the exact EC, we used Jensen's inequality to find out the upper bound of the Ergodic capacity. For completeness, the energy efficiency comparing the multi-IRS system to the reference single-IRS system is also discussed.
- Achieving reliability in the absence of a direct path between the BS and the UE is challenging. Thanks to the multi-IRS set-up, with the proposed model, we can improve the reliability at the UE by adjusting the number of reflecting elements at each IRS.
- Owing to the importance of the placement of the IRS in the vicinity of both BS and UE, at a fixed transmitted signal power we demonstrated the optimal placement of the IRS.
- Overall, the derived theoretical expressions and the mean Monte-Carlo (MC) simulated values are in good match and thus validated the proposed multi-IRS MIMO communication system under $\eta-\mu$ wireless channel environment. Through detailed analysis, we studied the importance of each parameter and discussed in length how those parameters effect the performance metric under consideration.

The structure of the paper unfolds as follows: Section II introduces the system model under consideration. In Section III, we delve into the performance analysis and present closed-form expressions. Section IV is dedicated to discussing the results obtained. Finally, Section V encapsulates the concluding remarks.

II. SYSTEM MODEL

In this article, we discuss a multi-IRS assisted MIMO system as depicted in Fig. 1, where the BS is equipped with Z_t number antennas and a UE with Z_r number antennas. Assuming a non-line-of-sight (NLOS) scenario between the BS and the UE, a low-cost efficient L multiple IRSs, placed at various locations and each IRS with N_k elements, are

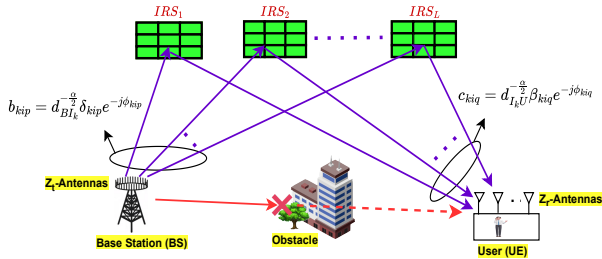


Fig. 1. Improved wireless connectivity using multiple antennas at the base station, user equipment, and multiple intelligent reflecting surfaces in non-line-of-sight scenarios.

employed to create a virtual LOS. The received signal at the UE is the superposition of all the reflected paths from each IRS and can be represented as [16],

$$y = \left[\sum_{k=1}^L \sum_{i=1}^{N_k} \sum_{p=1}^{Z_t} \sum_{q=1}^{Z_r} b_{kip} h_{ki} c_{kiq} \right] s + n \quad (1)$$

where s represents the data symbols chosen from the binary phase shift keying (BPSK) modulation scheme with average energy denoted as E_s . n corresponds to the additive white Gaussian noise (AWGN) characterized by a zero mean and a variance of N_o . $b_{kip} = d_{BI_k}^{-\frac{\alpha}{2}} \delta_{kip} e^{-j\phi_{kip}}$ and $c_{kiq} = d_{I_kU}^{-\frac{\alpha}{2}} \beta_{kiq} e^{-j\psi_{kiq}}$ are the channel coefficients from the p -th transmitting antenna to i -th element of the k -th IRS and the i -th element of the k -th IRS to the UE respectively, where d_{BI_k} and d_{I_kU} are the distance of BS to IRS, IRS to UE respectively, and also α is the mean path loss exponent. Moreover, δ_{kip} and β_{kiq} are the channel magnitudes, assumed in this study to follow the generalized $\eta - \mu$ fading distribution. ϕ_{kip} and ψ_{kiq} are the phases of BS to IRS and IRS to UE, respectively. h_{ki} in equation (1) is the reflection coefficient of the i -th element of the k -th IRS and is given by [12],

$$h_{ki} = a_{ki} e^{j\theta_{ki}}, \quad i = 1, 2, \dots, N_k \quad (2)$$

Here, a_{ki} and θ_{ki} denote the controllable gain and the phase factor at the i -th element of the k -th IRS, respectively. It is to be noted that depending upon the values of these parameters, $a_{ki} \in [0, 1]$ and $\theta_{ki} \in [0, 2\pi)$, the overall performance of the IRS-assisted communication system will be varied. For simplicity, in this work, we considered the optimal phase shift (OPS) choice of $\theta_{ki} = \phi_{kip} + \psi_{kiq}$ [21], to maximize the SNR at the UE. Nevertheless, given practical implementation, one can use discrete phase shift (DPS) to limit the number of discrete values chosen from a set of phase shifts in $[0, 2\pi)$ represented by $\theta_{ki} = \frac{2\pi}{2^b} f$, where $f = 0, 1, \dots, 2^b - 1$ and b is the number of digits to represent each level [22]. Assuming perfect reflection at the IRS, $|a_{ki}| = 1$, the received signal can be modified as follows,

$$y = \left[\sum_{k=1}^L \sum_{i=1}^{N_k} \sum_{p=1}^{Z_t} \sum_{q=1}^{Z_r} d_{BI_k}^{-\frac{\alpha}{2}} \delta_{kip} d_{I_kU}^{-\frac{\alpha}{2}} \beta_{kiq} \right] s + n \quad (3)$$

The maximum received SNR at the UE can be expressed as

TABLE I
 $\eta - \mu$ SPECIAL CASES

Description	η	μ
Rayleigh	1	0.5
Nakagami- m	1	$m/2$
Nakagami- q (Hoyt)	q^2	0.5

[12],

$$\begin{aligned} \gamma &= \frac{\left(\sum_{k=1}^L \sum_{i=1}^{N_k} \sum_{p=1}^{Z_t} \sum_{q=1}^{Z_r} d_{BI_k}^{-\frac{\alpha}{2}} \delta_{kip} d_{I_kU}^{-\frac{\alpha}{2}} \beta_{kiq} \right)^2 E_s}{N_o} \\ &= \frac{\Upsilon^2 E_s}{\left(\sum_{k=1}^L d_{BI_k}^\alpha d_{I_kU}^\alpha \right) N_o} = \Upsilon^2 \zeta \end{aligned} \quad (4)$$

where $\Upsilon = \left(\sum_{k=1}^L \sum_{i=1}^{N_k} \sum_{p=1}^{Z_t} \sum_{q=1}^{Z_r} \delta_{kip} \beta_{kiq} \right)$, $\zeta = \frac{E_s}{\left(\sum_{k=1}^L d_{BI_k}^\alpha d_{I_kU}^\alpha \right) N_o}$. As N_k is sufficiently large, according to the principle of the central limit theorem (CLT), Υ is expected to conform to a Gaussian distribution [23]. Consequently, γ will adhere to a non-central chi-squared (NCCS) distribution. Moreover, δ_{kip} and β_{kiq} in equation (3) are considered to be independent and identically distributed (IID) $\eta - \mu$ random variables, characterized by the following probability density function (PDF) [19], [24],

$$f_P(\rho) = \frac{2\sqrt{\pi}(1+\eta)^{\mu+\frac{1}{2}} \rho^{2\mu}}{\sqrt{\eta}(1-\eta)^{\mu-\frac{1}{2}} \Gamma(\mu)} \exp\left[-\frac{\mu(1+\eta)\rho^2}{2\eta}\right] I_{\mu-\frac{1}{2}}\left[\frac{\mu(1-\eta)\rho^2}{2\eta}\right] \quad (5)$$

where $\Gamma(\cdot)$ is the Gamma function, $I_n(\cdot)$ is the n -th modified Bessel function of the first kind, η represents the ratio of the non-centrality parameter to the scale parameter in the distribution. It essentially controls the spread or dispersion of the fading envelope. μ is associated with the shape parameter of the distribution. It influences the skewness of the fading envelope. The generalized $\eta - \mu$ fading distribution serves as a versatile model capable of encompassing a range of other distributions, such as Nakagami- m , Nakagami- q , and Rayleigh fading channels, as corner cases, as shown in Table I. It is particularly well-suited for NLOS environments, owing to its ability to capture the complex nature of propagation, including non-homogeneous conditions characterized by scattering elements, reflective surfaces, and diffraction phenomena.

The j -th moment of $\eta - \mu$ distribution is given as [19],

$$E(P^j) = \frac{2^{(2\mu+j/2)} \Gamma(2\mu+j/2)}{(2+\eta^{-1}+\eta)^{\mu+j/2} \mu^{j/2} \Gamma(2\mu)} {}_2F_1\left[\mu + \frac{j}{4} + \frac{1}{2}, \mu + \frac{j}{4}; \mu + \frac{1}{2}; \left(\frac{1-\eta}{1+\eta}\right)^2\right] \quad (6)$$

where ${}_2F_1(\cdot)$ is the Gauss hypergeometric function. Consequently, by utilizing equation (6), we can determine the mean and variance as follows,

$$\Delta_m \triangleq E(P) = \frac{2^{(2\mu+1/2)} \Gamma(2\mu+1/2)}{(2+\eta^{-1}+\eta)^{\mu+1/2} \mu^{1/2} \Gamma(2\mu)} {}_2F_1\left[\mu + \frac{3}{4}, \mu + \frac{1}{4}; \mu + \frac{1}{2}; \left(\frac{1-\eta}{1+\eta}\right)^2\right] \quad (7)$$

where $E(\cdot)$ is the expectation operator. The variance P is given in equation (8), where $\text{Var}(\cdot)$ is the variance operator (mentioned at the top of the next page).

$$\Delta_v \triangleq \text{Var}(P) = \left(\frac{4}{2 + \eta^{-1} + \eta} \right)^{\mu+1} {}_2F_1 \left[\mu + 1, \mu + \frac{1}{2}; \mu + \frac{1}{2}; \left(\frac{1 - \eta}{1 + \eta} \right)^2 \right] - \left[\frac{2^{(2\mu+1/2)} \Gamma(2\mu + 1/2)}{(2 + \eta^{-1} + \eta)^{\mu+1/2} \mu^{1/2} \Gamma(2\mu)} {}_2F_1 \left[\mu + \frac{3}{4}, \mu + \frac{1}{4}; \mu + \frac{1}{2}; \left(\frac{1 - \eta}{1 + \eta} \right)^2 \right] \right]^2 \quad (8)$$

III. PERFORMANCE ANALYSIS

In the forthcoming sub-sections that ensue, we formulate the analytical representations for BER, EC, and EE under the considered generalized framework. The statistical information of Υ is necessary to derive the analytical expressions of each of the performance metrics under consideration. With this, next we aim to find the mean and variance of Υ . Recalling δ_{kip} and β_{kiq} follow IID $\eta - \mu$ distribution functions, we have the following,

$$\text{E}[\delta_{kip}\beta_{kiq}] = \text{E}[\delta_{kip}] \text{E}[\beta_{kiq}] = \Delta_m^2 \quad (9)$$

$$\begin{aligned} \text{Var}[\delta_{kip}\beta_{kiq}] &= \text{Var}[\delta_{kip}] \text{Var}[\beta_{kiq}] + \text{Var}[\delta_{kip}] (\text{E}[\beta_{kiq}])^2 \\ &\quad + \text{Var}[\beta_{kiq}] (\text{E}[\delta_{kip}])^2 \\ &= \Delta_v^2 + 2\Delta_v \Delta_m^2 \end{aligned} \quad (10)$$

Consequently, Υ statistics can be derived as,

$$\Lambda_e \triangleq \text{E}[\Upsilon] = \text{E} \left[\sum_{k=1}^L \sum_{i=1}^{N_k} \sum_{p=1}^{Z_t} \sum_{q=1}^{Z_r} \delta_{kip}\beta_{kiq} \right] = LN_k Z_t Z_r \Delta_m^2 \quad (11)$$

$$\begin{aligned} \Lambda_v \triangleq \text{Var}[\Upsilon] &= \text{Var} \left[\sum_{k=1}^L \sum_{i=1}^{N_k} \sum_{p=1}^{Z_t} \sum_{q=1}^{Z_r} \delta_{kip}\beta_{kiq} \right] \\ &= LN_k Z_t Z_r (\Delta_v^2 + 2\Delta_v \Delta_m^2) \end{aligned} \quad (12)$$

A. Bit Error Rate

To derive the closed-form expression of BER, in this section, we follow a simple MGF approach. Since γ follows a NCCS distribution with one degree of freedom, the MGF can be expressed as [25],

$$\begin{aligned} M_\gamma(s) &= \text{E} \left[e^{s\Upsilon^2 \zeta} \right] \\ &= \int_{-\infty}^{\infty} e^{s(\Upsilon^2 \zeta)} f_\Upsilon(\Upsilon) d\Upsilon \\ &= \int_{-\infty}^{\infty} e^{s(\Upsilon^2 \zeta)} \frac{1}{\sqrt{2\pi\Lambda_v^2}} e^{-\frac{(\Upsilon - \Lambda_e)^2}{2\Lambda_v^2}} d\Upsilon \\ &= \frac{e^{-\frac{\Lambda_e^2}{2\Lambda_v^2}}}{\sqrt{2\pi\Lambda_v^2}} \int_{-\infty}^{\infty} \exp \left\{ - \left(\frac{1}{2\Lambda_v^2} - s\zeta \right) \Upsilon^2 + \frac{\Upsilon\Lambda_e}{\Lambda_v^2} \right\} d\Upsilon \\ &= \frac{e^{-\frac{\Lambda_e^2}{2\Lambda_v^2}} e^{\frac{\Lambda_e^2}{2\Lambda_v^2(1-s\zeta 2\Lambda_v^2)}}}{\sqrt{2\pi\Lambda_v^2}} \int_{-\infty}^{\infty} \exp \left\{ - \left[\Upsilon - \frac{\Lambda_e}{(1-s\zeta 2\Lambda_v^2)} \right]^2 \right\} \frac{1}{2\Lambda_v^2 (1-s\zeta 2\Lambda_v^2)^{-1}} d\Upsilon \end{aligned}$$

$$M_\gamma(s) = \left(\frac{1}{1 - \frac{2s\Lambda_v E_s}{d_{B I_k}^\alpha d_{I_k U}^\alpha N_o}} \right)^{\frac{1}{2}} \exp \left(\frac{\frac{s\Lambda_e^2 E_s}{d_{B I_k}^\alpha d_{I_k U}^\alpha N_o}}{1 - \frac{2s\Lambda_v E_s}{d_{B I_k}^\alpha d_{I_k U}^\alpha N_o}} \right) \quad (13)$$

The average SER of M -PSK signaling is calculated as [25],

$$P_e = \frac{1}{\pi} \int_0^{\frac{(M-1)\pi}{M}} M_\gamma \left(\frac{-\sin^2(\pi/M)}{\sin^2 v} \right) dv \quad (14)$$

For $M = 2$ binary PSK, equation (14) simplifies to,

$$P_e = \frac{1}{\pi} \int_0^{\frac{\pi}{2}} \left(\frac{1}{1 + \frac{2\Lambda_v E_s}{d_{B I_k}^\alpha d_{I_k U}^\alpha N_o \sin^2 v}} \right)^{\frac{1}{2}} \exp \left(\frac{-\Lambda_e^2 E_s}{1 + \frac{2\Lambda_v E_s}{d_{B I_k}^\alpha d_{I_k U}^\alpha N_o \sin^2 v}} \right) dv \quad (15)$$

To solve problem equation (15), expanding exponential series and following [[26],3.681], the probability of error rate is given as,

$$\begin{aligned} P_e &= \frac{1}{\pi} \sum_{n=0}^{\infty} \frac{\left(\frac{-\Lambda_e^2 E_s}{d_{B I_k}^\alpha d_{I_k U}^\alpha N_o} \right)^n \left(\frac{2\Lambda_v E_s}{d_{B I_k}^\alpha d_{I_k U}^\alpha N_o} \right)^{\frac{1}{2}-n}}{n! \left(1 + \frac{2\Lambda_v E_s}{d_{B I_k}^\alpha d_{I_k U}^\alpha N_o} \right)} \\ &\quad * {}_2F_1 \left[1, 1 - n, \frac{3}{2}, \frac{1}{1 + \frac{2\Lambda_v E_s}{d_{B I_k}^\alpha d_{I_k U}^\alpha N_o}} \right] \end{aligned} \quad (16)$$

Even though the probability of error expression consists of an infinite series, it is observed that less than ten terms are sufficient to get the desired accuracy of the SER performance. This indicates that the series converges quickly to get the desired error rates of 10^{-5} [27].

B. Ergodic Capacity

Typically, the EC in the context of a fading channel is expressed as follows [23],

$$C = \text{E}[\log_2(1 + \gamma)] \quad (17)$$

Given that γ follows the NCCS distribution with one degree of freedom, deriving the closed-form EC expression is quite challenging. Therefore, employing Jensen's inequality, we establish the upper bound of equation (17) given as [28],

$$C_{UP} = \log_2(1 + \text{E}[\gamma]) \quad (18)$$

From (4), $\text{E}[\gamma] = \text{E}[\Upsilon^2 \zeta] = \zeta \text{E}[\Upsilon^2]$. Using the definition of variance, $\text{E}[\Upsilon^2] = \text{Var}[\Upsilon] + [\text{E}[\Upsilon]]^2$ we have the following,

$$\text{E}[\gamma] = \zeta \left(\text{Var}[\Upsilon] + [\text{E}[\Upsilon]]^2 \right) \quad (19)$$

Accordingly, C_{UP} can be rewritten as,

$$C_{UP} = \log_2 \left(1 + \zeta \left(\text{Var}[\Upsilon] + [\text{E}[\Upsilon]]^2 \right) \right) \quad (20)$$

TABLE II
SIMULATION PARAMETERS [18], [29]

Description	Values
Number of reflecting elements, N	16 – 512
Distance between BS to UE, d [m]	100
Height of IRS (h_{IRS}) [m]	15
Height of BS (h_{BS}) [m]	10
Height of UE (h_{UE}) [m]	2
Path loss Exponent, α	3
Carrier frequency (f_c) [GHz]	3
Transmit power (P_s) [dBm]	[0, 30]
Power dissipated, P_{ik} [mW]	7.8
Power conversion efficiency (ξ)	80%
Circuit dissipated power at BS (P_c^{BS}) [dBm]	10
Circuit dissipated power at UE (P_c^{UE}) [dBm]	10
Bandwidth (BW) [MHz]	10
Noise Figure (NF) [dBm]	10
Modulation scheme	BPSK

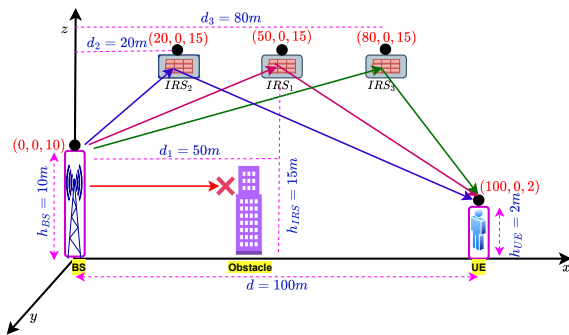


Fig. 2. Simulation setup of the proposed system model in NLOS scenarios using multiple antennas at both the base station, user equipment, and multiple IRSs.

Now using equation (11), the upper bound for the EC can be written as,

$$C_{UP} = \log_2 (1 + \zeta (\Lambda_v + \Lambda_e^2)) \quad (21)$$

C. Energy Efficiency

The energy efficiency (EE) of a system aided by an IRS can be elucidated as [18],

$$EE = B \times \left(\frac{R}{P_{total}} \right) \quad (22)$$

Here, B represents the bandwidth, while R signifies the target spectral efficiency. P_{total} represents the total power of the system, which can be computed as [18], [29],

$$P_{total} = P_s + P_s^{HPA} + P_c^{BS} + LN_k P_{ik} + P_c^{UE} \quad (23)$$

Here, P_s represents the transmit power at the BS, $P_s^{HPA} = \frac{P_s}{\xi}$ is the power utilized by the high-power amplifier (HPA) with ξ being the efficiency of power conversion [30], P_c^{BS} is circuit dissipated power at the BS, P_{ik} is the power dissipated at the i^{th} IRS element of the k^{th} IRS, and P_c^{UE} is circuit dissipated power at UE.

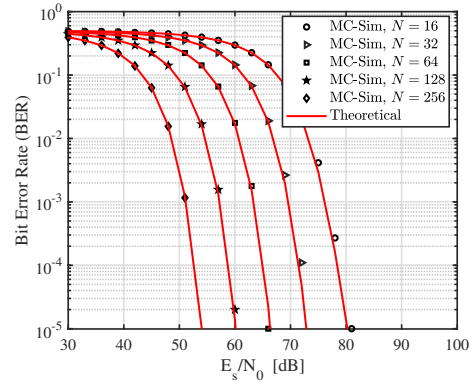


Fig. 3. BER versus SNR performance using binary phase shift keying (BPSK) signalling for varying N with $Z_t = Z_r = 2$, $\eta = 1$, $\mu = 0.5$, and S-IRS.

IV. RESULTS AND DISCUSSIONS

In this section, we provide the results of the derived BER, EC, and EE of the system model under consideration for single-IRS (S-IRS), double-IRS (D-IRS), and triple-IRS (T-IRS). A mean Monte-Carlo (MC) simulation set-up is made according to the parameter setting in Table II, not only to verify the correctness of the derived analytical expressions but also to get more insights about the variables affecting the overall system performance. The comparison among multiple IRSs is conducted by ensuring the number of reflecting elements in S-IRS, D-IRS, and T-IRS systems were all equal to N , specifically i.e. $N_1 = 2N_2 = 3N_3 = N$, where N_1 , N_2 , and N_3 as the numbers of reflecting elements in the S-IRS, D-IRS, and T-IRS, respectively. The simulation set-up is made according to Fig. 2.

In the following subsections, we have detailed the effect of the number of reflecting elements and distance parameters on each of the performance metrics. However, this analysis was carried out assuming the impact of the other parameters chosen in Table II as constant. In brief, we would like to highlight the following points:

- Increasing the heights h_{BS} or h_{UE} will improve the overall performance since the IRSs will be closer to both the BS and the UE which inturn increases the received signal strength.
- Increasing the h_{IRS} will degrade the performance of the considered system model as the received signal strength at the UE will be reduced due to farther distance from the IRSs.
- From equation (4), we can conclude that increasing the value of path-loss will reduce the γ value and hence will degrade the system performance.
- Also, from (22) we can observe that the P_{total} is a function of P_s , P_s^{HPA} , P_c^{BS} , P_{ik} , and, P_c^{UE} . We can observe that an increase or decrease in the values of these power components will reduce or enhance the performance respectively.

A. BER Results

Figure 3 presents a comparison between the theoretical, and simulated results by fixing $\eta = 1$, $\mu = 0.5$ for the various number of reflecting elements, $N \in \{16, 32, 64, 128, 256\}$. It can be noted that in accordance with Table I, this fading parameter setting boils down the system model to the Rayleigh channel. The following insights can be observed:

- As the value of N increases, the precision of both the theoretical and MC simulated results remains consistent. The reason for this can be attributed to the fact that the analytical expressions derived in Section III rely on the CLT assumption. Consequently, a larger value of N results in a more accurate Gaussian approximation and more tightness of the derived expression and the MC simulations.
- The reliability of an IRS-supported communication system can be improved by increasing the number of reflecting elements. For example, at an $E_s/N_0 = 60$ dB, the BER values are 10^{-5} , 0.01, 0.14, and 0.29 for $N \in \{128, 64, 32, 16\}$ respectively. This implies that low-cost energy efficient passive IRS elements play a crucial role in improving the reliability of the information.
- On the contrary, to achieve a fixed BER, an increase in the number of reflecting elements can be traded off with the E_s/N_0 . As an example, to attain a BER value of 10^{-4} , the E_s/N_0 required is approximately 80 dB, 71 dB, 65 dB, 59 dB, and 52 dB for $N \in \{16, 32, 64, 128, 256\}$ respectively. This implies that depending upon the resources available at the BS, the number of reflecting elements can be traded off.

In Fig. 4(a), the BER performance is illustrated by varying the parameter μ for a fixed $\eta = 1$. This simulation parameter setting covers the Nakagami- m fading channel as a special case which is reflected in Table I. The analytical expression and MC simulated results agree, and as μ increases, the BER decreases due to the quantity of multipath clusters. For instance, when μ value increases from 0.5 to 1.5, a gain of ≈ 2 dB is achieved at a fixed BER of 10^{-5} . Fig. 4(b) shows the impact of fading parameter η for a fixed $\mu = 0.5$, covering the Nakagami- q fading channel as per Table I. The BER expression matches the simulated results, showing that an increase in η decreases the error rate, as it enhances the power of dominant waves.

Fig. 5(a) illustrates the comparison of BER performance between OPS, DPS, and random phase shift (RPS). The choice of OPS is clearly understood to yield the optimal BER performance, as it assumes perfect phase compensation. Conversely, if the IRS elements phase shift values are randomly selected from the range $[0, 2\pi)$, the BER performance of the RPS becomes less dependable. Curiously, the DPS will be closer to the optimal choice depending on the value of b . It is observed that the BER performance for 3-bit level phase shifts is nearly equivalent to that of the OPS case. Quantitatively, at E_s/N_0 of 70 dB the BER values are 0.0001, 0.0001, 0.0007, 0.0444, and 0.2569 respectively for OPS, DPS ($b = 3$), DPS ($b = 2$), DPS ($b = 1$), and RPS.

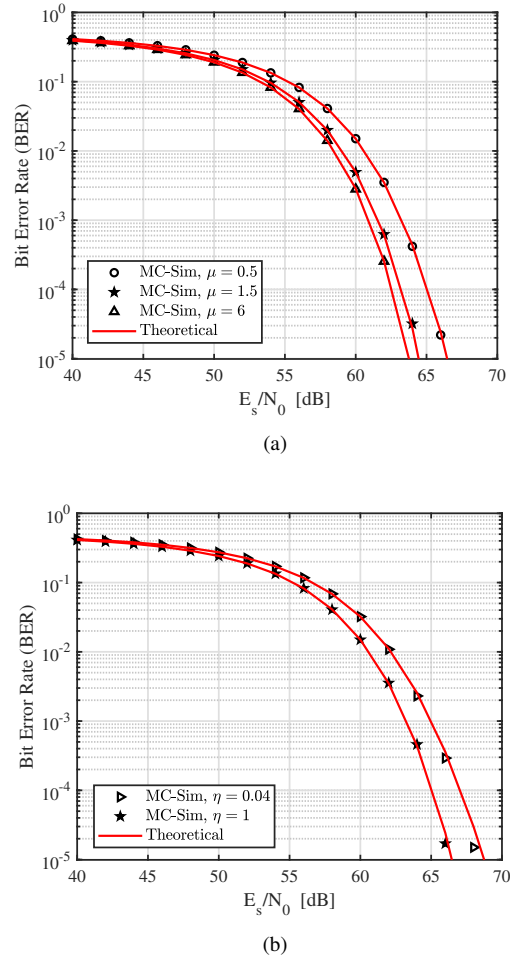


Fig. 4. BER versus SNR analysis with varying fading parameters (a) $\eta = 1$, $Z_t = Z_r = 1$, $N = 64$, S-IRS (b) $\mu = 0.5$, $Z_t = Z_r = 1$, $N = 64$, S-IRS

Fig. 5(b) demonstrates the influence of the placements of IRSs on the BER of the D-IRS system by altering the number of antennas at BS and UE, denoted as Z_t and Z_r . The improvement in the BER performance of the D-IRS system is clearly observed when IRS₁ and IRS₂ are positioned in greater proximity to the BS and UE, respectively. In addition, as expected increasing the number of antennas will decrease the BER.

Fig. 6(a) displays the BER performance of a multi-IRS system. The theoretical expressions discussed in Section III matches exactly with the mean Monte-Carlo simulations. For a fair comparison, we set $N_1 = 150$ for S-IRS, while D-IRS has two IRSs positioned consecutively along the BS-UE route, each configured with N_1 and N_2 set to 75, and T-IRS has three IRSs positioned consecutively along the BS-UE route, each configured with N_1 , N_2 , and N_3 set to 50. The plot shows that increasing the number of IRSs along the path leads to improved system reliability. A gain of 4 dB and 6 dB are observed at a BER of 10^{-5} when the number of IRS stages changes from S-IRS to D-IRS and D-IRS to T-IRS, respectively.

Fig. 6(b) compares the theoretical and simulated results of

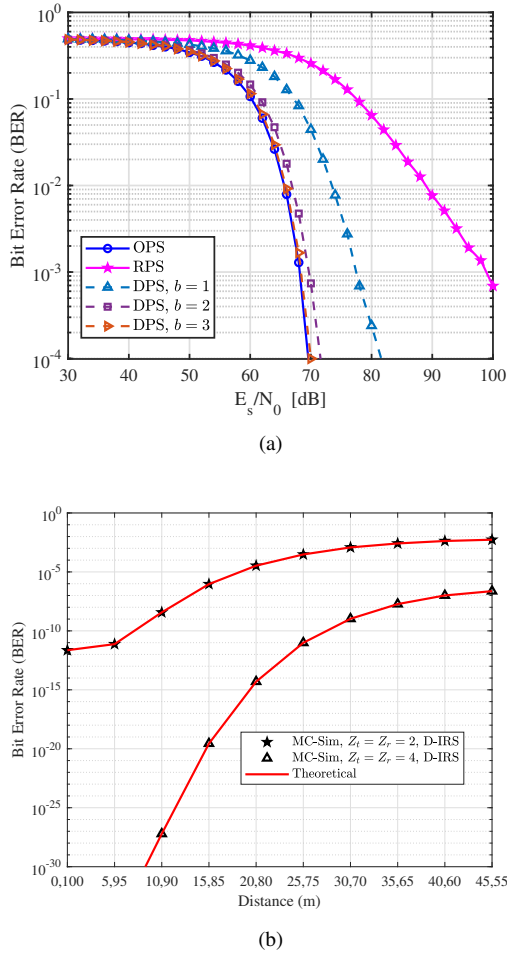


Fig. 5. (a) BER versus SNR analysis for different phase schemes with $N = 32$, $Z_t = Z_r = 1$, $\eta = 1$, $\mu = 1$, and S-IRS. (b) BER versus distance for fixed $E_s/N_0 = 50$ dB, $\eta = 1$, $\mu = 0.5$, $N = 240$.

a multi-IRS assisted system for various number of antennas at the BS, UE $(Z_t, Z_r) \in \{(2, 2), (4, 2), (4, 4), (6, 6)\}$. Increasing the number of antennas at the BS can significantly improve the BER performance. For example, at E_s/N_0 of 30 dB the BER values are 0.3146, 0.1673, 0.0267, and 0.00021 respectively for $(Z_t, Z_r) \in \{(2, 2), (4, 2), (4, 4), (6, 6)\}$.

Fig. 7 illustrates the comparison of the BER performance between SISO, MISO, and MIMO. From the plot, one can observe that employing multiple antennas decreases the error rates providing an improved reliable system. This can be justified by the fact that by using multiple antenna systems, the signal can follow multiple independent paths resulting in an improved BER performance. The theoretical expressions discussed in Section III match exactly the mean Monte-Carlo simulations. An improvement of around 10 dB is observed when switching from SISO to MISO and from MISO to MIMO at a BER of 10^{-4} .

B. EC Results

In Fig. 8(a), the effect of the location of IRS on the EC is plotted for a fixed $P_s = 10$ dBm, and fading parameters $\eta=1$ and $\mu = 0.5$. It can be noted that this setting boils down

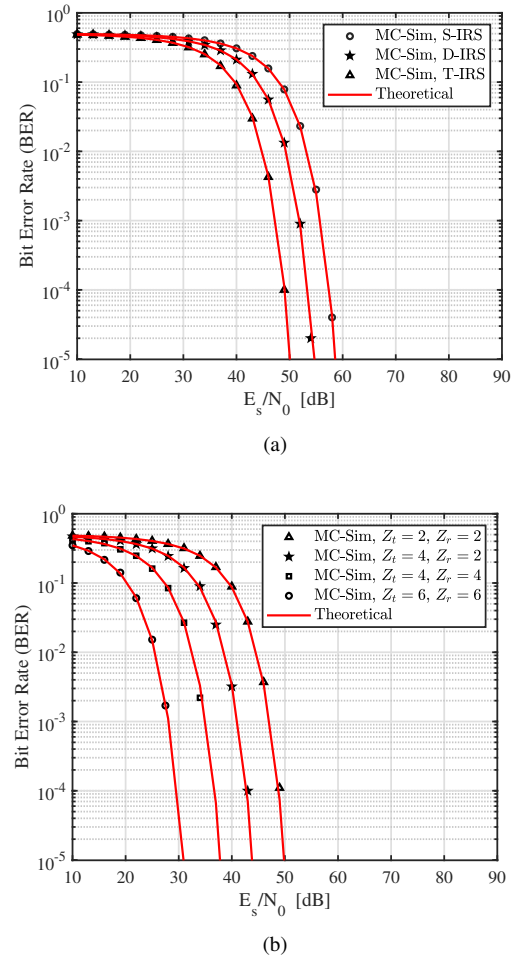


Fig. 6. BER versus SNR performance using BPSK signalling with $\eta = 1$, $\mu = 0.5$ (a) $N = 150$, $Z_t = Z_r = 2$, varying multiple-IRS (b) D-IRS, $N = 256$, varying Z_t, Z_r .

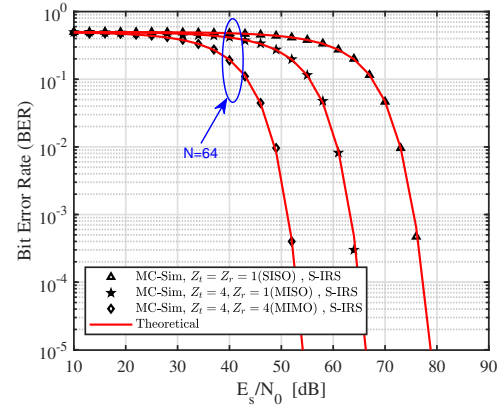


Fig. 7. ER versus SNR performance using binary phase shift keying (BPSK) signalling for varying Z_t, Z_r with $N = 64$, $\eta = 1$, $\mu = 0.5$, and S-IRS.

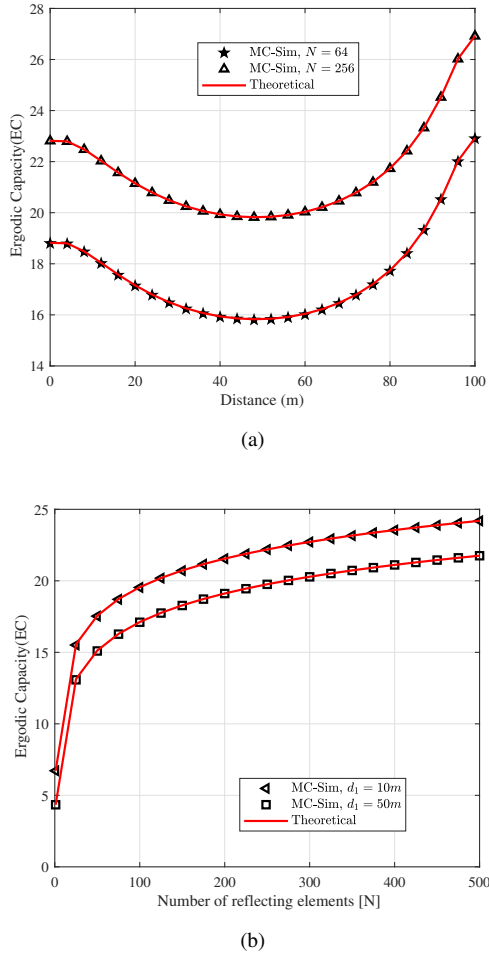


Fig. 8. (a) EC versus Distance analysis with fixed $P_s=10$ dBm, $\eta=1$, $\mu = 0.5$, $Z_t = Z_r=2$, S-IRS for varying N (b) EC versus N analysis with fixed $P_s=10$ dBm, $\eta=1$, $\mu = 0.5$, $Z_t = Z_r=2$, S-IRS for varying d_1 .

to the EC analysis under Rayleigh fading channel. Similar to the observations made from other performance metrics, the achievable rate is maximum when the IRS is closer to either BS or UE. Interestingly, the attainable EC remains constant when the IRS is positioned in a similar location to both the BS and the UE. For instance, when the distance between the IRS and the BS as well as the distance between the IRS and the UE is 40m, a capacity value of 16 (b/s/Hz) is achieved with $N = 64$. In addition, the EC reaches to minimum exactly when the IRS is at the midpoint of BS and UE. Lastly, the EC values increase when the N value increases.

Fig. 8(b) shows Ergodic capacity versus N , for varying d_1 with fixed $P_s = 10$ dBm, $\eta = 1$ and $\mu = 0.5$. From this plot, we can observe that the EC values increase exponentially in accordance with the number of reflecting elements. For example, with $N = 300$, the EC values of 20.27, and 22.71 b/s/Hz are achieved when IRS is 50m, and 10m away from BS respectively.

Fig. 9(a) illustrates the benefit of multiple-IRSs on the EC performance. The illustration shows that as the transmit power P_s increases, the EC of the system also increases for a constant

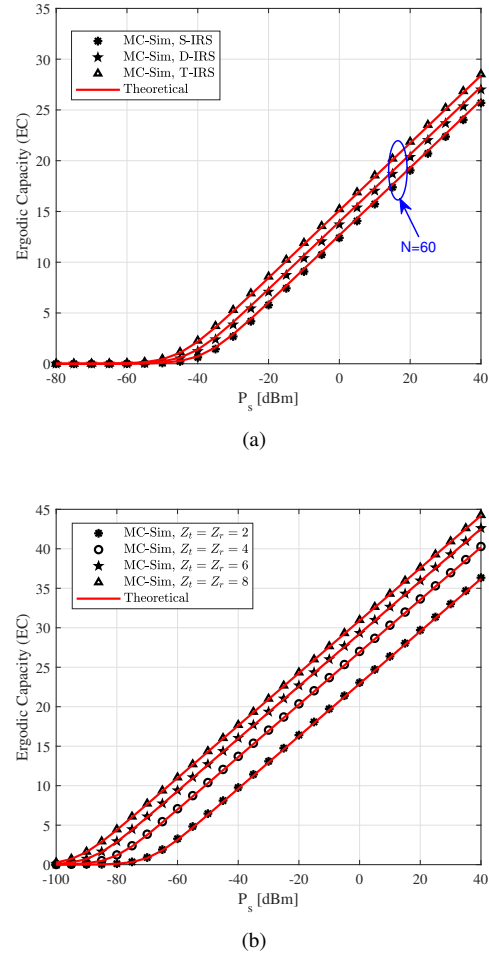


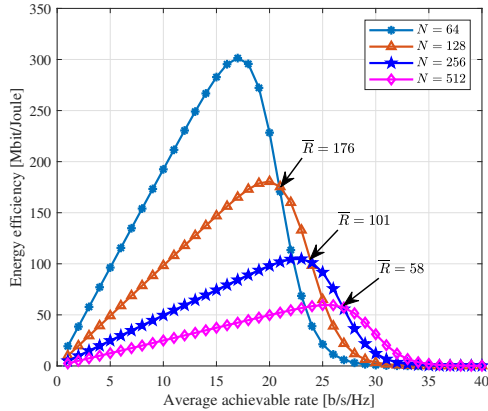
Fig. 9. Ergodic capacity versus source transmit power, P_s , with (a) $\eta = 1$, $\mu = 1$, $N = 60$, $Z_t = Z_r=2$ (b) $N = 300$, $\eta = 1, \mu = 1$, and T-IRS.

N value. This phenomenon arises due to an increased P_s , resulting in an enhanced signal at the UE. As a result, the ability to transmit a larger amount of information reliably is enhanced. As anticipated, when the value of N remains constant, the EC of the systems exhibits a growth pattern (T-IRS > D-IRS > S-IRS) that corresponds to the increase in transmit power P_s . Based on the observations from Fig. 9(a), we can conclude that the upper bound derived in Section III-B aligns well with the simulated results for the multi-IRS scenario.

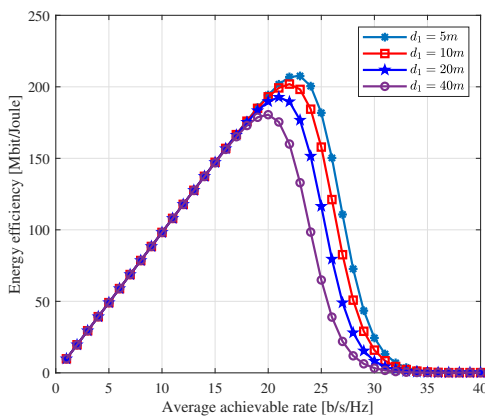
Fig. 9(b), we analyze the effect of the number of antenna elements (Z_t, Z_r) on the EC in the presence of multi-IRS. As the transmit power P_s increases, the EC of the system also increases proportionally for a given Z_t, Z_r values. For example, at a fixed value of $P_s = 40$ dBm, for the T-IRS system, the attainable EC values are 36.34, 40.19, 42.53, and 44.19 (b/s/Hz), corresponding to (Z_t, Z_r) values of (2, 2), (4, 4), (6, 6), and (8, 8), respectively.

C. EE Results

In Fig. 10(a), the EE that can be attained for a target achievable rate is studied in accordance with the equation



(a)



(b)

Fig. 10. Energy efficiency versus average achievable rate (a) for varying N with fixed $\eta = 1$, $\mu = 1.5$, $Z_t = Z_r = 2$, S-IRS (b) for varying d_1 with fixed $\eta = 1$, $\mu = 0.5$, $N = 128$, $Z_t = Z_r = 2$, S-IRS.

(22). From the plot, we can notice that for low data rates with $\bar{R} = 176$ b/s/Hz, where \bar{R} represents the crossing point, $N = 64$ is a better EE system compared to $N = 128$. In addition, when higher data rates are required, $N = 128$ results in a better EE system than $N = 64$. A similar observation can be made when $N = 128$ and \bar{R} being 101 b/s/Hz as illustrated in Fig. 10(a). In short, for low data rate applications, the lesser the N value, the better the EE, and for high data rate applications vice-versa. Comparing Fig. 8(b) and Fig. 10(a) we can get some insights in terms of the practical design perspective. For instance, as shown in Fig. 8(b), increasing the number of IRS elements significantly enhances EC, making it ideal for high-capacity systems, while smaller N values are better suited for energy-constrained scenarios as indicated in Fig. 10(a). Hence depending on the requirement, a trade-off can be chosen by the designer between the EC and EE.

The effect of distance on the achievable rate is shown in Fig. 10(b). The position of the IRS highly influences the capacity of the system. To be precise, the closer the location of the IRS to BS higher the value of the EC. For instance, to achieve a rate of 25 b/s/Hz, the EE (in Mbits/Joule) obtained

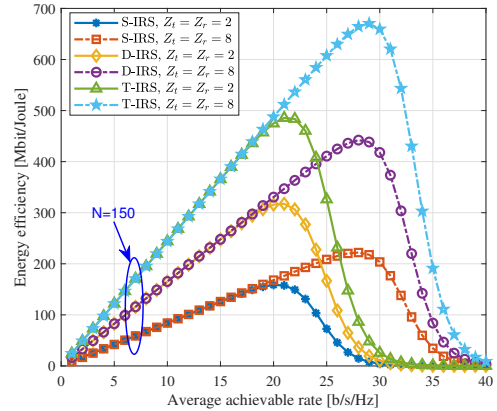


Fig. 11. Energy efficiency versus average achievable rate for varying Z_t, Z_r with fixed $\eta = 1$, $\mu = 0.5$.

at $d_1 \in \{5, 10, 20, 40\}$ m are $\{181.81, 157.87, 116.49, 64.91\}$ respectively. This suggests that the IRS's placement helps in designing a green communication system in terms of EE.

Fig. 11, considering the total power consumption which is a superposition of circuit power dissipation of both the BS, UE, and hardware impairments of IRS elements, we assess the EE of S-IRS, D-IRS, and T-IRS systems with same number of reflecting elements with the target spectral efficiency (R) with respect to equation (22). Firstly, the T-IRS system outperforms the D-IRS and S-IRS systems for a fixed average achievable rate. For instance, to achieve a rate of 25 b/s/Hz with $(Z_t, Z_r) = (8, 8)$, the EE (in Mbits/Joule) obtained at S-IRS, D-IRS, and T-IRS are 208.51, 410.8, and 607.65 respectively. In addition, for high values of achievable rate, employing multiple-IRSs is more beneficial than the S-IRS system. Secondly, for a fixed number of IRSs, when the number of antennas at the BS increases the the energy efficiency increases to achieve the same achievable rate. For example, to achieve a rate of 25 b/s/Hz for D-IRS with $(Z_t, Z_r) \in \{(2, 2), (8, 8)\}$, the EE values are 166.58 and 410.8 respectively. The above two observations can be justified by the fact that, in accordance with the discussion of the results in Section III-B, the T-IRS achieves a better rate compared to D-IRS and S-IRS and can be traded off with the target average achievable rate with the energy efficiency in equation (22).

V. CONCLUSIONS

In this article, we analyzed the BER, EC, and EE performance analysis of a multi-antenna multi-IRS assisted communication system assuming the envelope of all the channel links follows a generalized $\eta - \mu$ distribution. By applying CLT, the statistical information of the received SNR for the system under consideration has been derived in terms of first-order and second-order moments. Thus, due to this, the closed-form theoretical expressions of BER, and upper bound of EC were evaluated. The exactness of the analytical expressions is validated through the MC simulated results and is intact for large values of reflecting elements. Further, the derived expressions cover Rayleigh, Nakagami- m , and Nakagami- q fading channels as corner cases. Under the same simulation

setup, after rigorous analysis, we found that a multi-IRS system offers an enhanced performance compared to the S-IRS system. In addition, we also focus on the EE of the overall system is discussed in length and we observed that the T-IRS system outperforms D-IRS and S-IRS systems. It has been noted that increasing the number of antennas at the BS and UE, the number of IRSs between the transceiver link, the number of reflecting elements, and the placement of the IRS plays a vital role in the optimal performance of the considered system model. Also, the interplay between the tradeoff of the stakeholder parameters depending upon the resources available at disposal is discussed. In brief, low-cost reflecting elements can be used to achieve the target BER with low SNR values and the target EC, multi-IRSs in the vicinity of either BS or UE can be employed to high energy efficiency which can be traded with the transmit power at the BS. In conclusion, a more generalized system model has been considered under the $\eta - \mu$ fading channel to cover a wide range of scenarios, which can be integrated with the existing wireless networks.

REFERENCES

- [1] Y. Liu, X. Liu, X. Mu, T. Hou, J. Xu, M. Di Renzo, and N. Al-Dhahir, "Reconfigurable intelligent surfaces: Principles and opportunities," *IEEE communications surveys & tutorials*, vol. 23, no. 3, pp. 1546–1577, 2021, doi:10.1109/COMST.2021.3077737.
- [2] F. A. P. de Figueiredo, "An overview of massive mimo for 5g and 6g," *IEEE Latin America Transactions*, vol. 20, no. 6, pp. 931–940, 2022, doi:10.1109/TLA.2022.9757375.
- [3] Q. Wu, S. Zhang, B. Zheng, C. You, and R. Zhang, "Intelligent reflecting surface-aided wireless communications: A tutorial," *IEEE transactions on communications*, vol. 69, no. 5, pp. 3313–3351, 2021, doi:10.1109/TCOMM.2021.3051897.
- [4] M. A. ElMossallamy, H. Zhang, L. Song, K. G. Seddik, Z. Han, and G. Y. Li, "Reconfigurable intelligent surfaces for wireless communications: Principles, challenges, and opportunities," *IEEE Transactions on Cognitive Communications and Networking*, vol. 6, no. 3, pp. 990–1002, 2020, doi:10.1109/TCCN.2020.2992604.
- [5] S. Gong, X. Lu, D. T. Hoang, D. Niyato, L. Shu, D. I. Kim, and Y.-C. Liang, "Toward smart wireless communications via intelligent reflecting surfaces: A contemporary survey," *IEEE Communications Surveys & Tutorials*, vol. 22, no. 4, pp. 2283–2314, 2020, doi:10.1109/COMST.2020.3004197.
- [6] E. Björnson, Ö. Özdogan, and E. G. Larsson, "Intelligent reflecting surface versus decode-and-forward: How large surfaces are needed to beat relaying?" *IEEE Wireless Communications Letters*, vol. 9, no. 2, pp. 244–248, 2019, doi:10.1109/LWC.2019.2950624.
- [7] Ö. Özdogan, E. Björnson, and E. G. Larsson, "Intelligent reflecting surfaces: Physics, propagation, and pathloss modeling," *IEEE Wireless Communications Letters*, vol. 9, no. 5, pp. 581–585, 2019, doi:10.1109/LWC.2019.2960779.
- [8] Y. J. Chun, S. L. Cotton, H. S. Dhillon, F. J. Lopez-Martinez, J. F. Paris, and S. K. Yoo, "A comprehensive analysis of 5g heterogeneous cellular systems operating over $\kappa - \mu$ shadowed fading channels," *IEEE Transactions on Wireless Communications*, vol. 16, no. 11, pp. 6995–7010, 2017, doi:10.1109/TWC.2017.2734080.
- [9] S. Li, B. Duo, X. Yuan, Y.-C. Liang, and M. Di Renzo, "Reconfigurable intelligent surface assisted uav communication: Joint trajectory design and passive beamforming," *IEEE Wireless Communications Letters*, vol. 9, no. 5, pp. 716–720, 2020, doi:10.1109/LWC.2020.2966705.
- [10] Z. Chen, X. Ma, C. Han, and Q. Wen, "Towards intelligent reflecting surface empowered 6g terahertz communications: A survey," *China Communications*, vol. 18, no. 5, pp. 93–119, 2021, doi:10.23919/JCC.2021.05.007.
- [11] A. M. Salhab and M. H. Samuh, "Accurate performance analysis of reconfigurable intelligent surfaces over rician fading channels," *IEEE Wireless Communications Letters*, vol. 10, no. 5, pp. 1051–1055, 2021, doi:10.1109/LWC.2021.3056758.
- [12] E. Basar, "Transmission through large intelligent surfaces: A new frontier in wireless communications," in *2019 European Conference on Networks and Communications (EuCNC)*. IEEE, 2019, pp. 112–117, doi:10.1109/EuCNC.2019.8801961.
- [13] S. Penchala, M. Chaudhary, S. K. Bandari, and V. V. Mani, "Impact of nakagami-m fading channel on reconfigurable intelligent surface symbol error rate in non-line-of-sight scenarios," in *IEEE 19th India Council International Conference (INDICON)*, Kochi, India, 2022, pp. 1–4, doi:10.1109/INDICON56171.2022.10040187.
- [14] R. Mahammad Rafi and V. Sudha, "Double reconfigurable intelligent surface to improve error performance and coverage probability of wireless communication system," *IETE Journal of Research*, pp. 1–10, 2023, doi:10.1080/03772063.2023.2258533.
- [15] S. Penchala, S. K. Bandari, V. Mani, and S. K. Kondoju, "On the bit error rate analysis of log-normal fading channel in irs-setup," in *2023 IEEE 20th India Council International Conference (INDICON)*, 2023, pp. 209–213, doi:10.1109/INDICON59947.2023.10440835.
- [16] L. Yang, Y. Yang, D. B. d. Costa, and I. Trigui, "Outage probability and capacity scaling law of multiple ris-aided networks," *IEEE Wireless Communications Letters*, vol. 10, no. 2, pp. 256–260, 2021, doi:10.1109/LWC.2020.3026712.
- [17] I. Yildirim, A. Uyrus, and E. Basar, "Modeling and analysis of reconfigurable intelligent surfaces for indoor and outdoor applications in future wireless networks," *IEEE transactions on communications*, vol. 69, no. 2, pp. 1290–1301, 2020, doi:10.1109/TCOMM.2020.3035391.
- [18] T. N. Do, G. Kaddoum, T. L. Nguyen, D. B. Da Costa, and Z. J. Haas, "Multi-ris-aided wireless systems: Statistical characterization and performance analysis," *IEEE Transactions on Communications*, vol. 69, no. 12, pp. 8641–8658, 2021, doi:10.1109/TCOMM.2021.3117599.
- [19] M. D. Yacoub, "The $\kappa - \mu$ distribution and the $\eta - \mu$ distribution," *IEEE Antennas and Propagation Magazine*, vol. 49, no. 1, pp. 68–81, 2007, doi:10.1109/MAP.2007.370983.
- [20] G. R. De Lima Tejerina, C. R. N. da Silva, R. A. A. de Souza, and M. D. Yacoub, "On the extended $\eta - \mu$ model: New results and applications to irs-aided systems," *IEEE Transactions on Vehicular Technology*, vol. 72, no. 4, pp. 4133–4142, 2022, doi:10.1109/TVT.2022.3222064.
- [21] P. Nayeri, F. Yang, and A. Z. Elsherbini, "Reflectarray antennas: theory, designs, and applications," 2018.
- [22] Q. Wu and R. Zhang, "Beamforming optimization for wireless network aided by intelligent reflecting surface with discrete phase shifts," *IEEE Transactions on Communications*, vol. 68, no. 3, pp. 1838–1851, 2019, doi:10.1109/TCOMM.2019.2958916.
- [23] J. Proakis and M. Salehi, "Digital communications 5th edition mcgraw-hill," *New York*, 2008.
- [24] S. K. Bandari, S. S. Yadav, and V. Mani, "Analysis of gfdm in generalized $\eta - \mu$ fading channel: A simple probability density function approach for beyond 5g wireless applications," *AEU-International Journal of Electronics and Communications*, vol. 153, p. 154260, 2022, doi:10.1016/j.aeue.2022.154260.
- [25] M. Simon, "Alouini. ms: Digital communication over fading channels," *A John Wiley Sons.-2005.-900 p*, 2005, doi:10.1109/TIT.2008.924676.
- [26] I. S. Gradshteyn and I. M. Ryzhik, "Table of integrals, series, and products," *Academic press*, 2014, doi:10.1016/C2010-0-64839-5.
- [27] H. Ji, S. Park, J. Yeo, Y. Kim, J. Lee, and B. Shim, "Ultra-reliable and low-latency communications in 5g downlink: Physical layer aspects," *IEEE Wireless Communications*, vol. 25, no. 3, pp. 124–130, 2018.
- [28] Q. Zhang, S. Jin, K.-K. Wong, H. Zhu, and M. Matthaiou, "Power scaling of uplink massive mimo systems with arbitrary-rank channel means," *IEEE Journal of Selected Topics in Signal Processing*, vol. 8, no. 5, pp. 966–981, 2014, doi:10.1109/JSTSP.2014.2324534.
- [29] M. H. N. Shaikh, V. A. Bohara, A. Srivastava, and G. Ghatak, "Performance analysis of intelligent reflecting surface-assisted wireless system with non-ideal transceiver," *IEEE Open Journal of the Communications Society*, vol. 2, pp. 671–686, 2021, doi:10.1109/OJCOMS.2021.3068866.
- [30] Z. Yao, W. Cheng, W. Zhang, and H. Zhang, "Resource allocation for 5g-uav-based emergency wireless communications," *IEEE Journal on Selected Areas in Communications*, vol. 39, no. 11, pp. 3395–3410, 2021, doi:10.1109/JSAC.2021.3088684.



Suresh Penchala received his B.Tech and M.Tech degrees in Electronics and Communication Engineering from JNTU Hyderabad, Telangana, India, in 2005 and 2008 respectively. He is currently pursuing a Ph.D. degree at the National Institute of Technology, Meghalaya, India. His research interests include intelligent Reflecting Surfaces, wireless communication beyond 5G, and signal processing for communication. He is an associate member of the Institute of Electronics and Telecommunication Engineers (IETE), India.



Shravan Kumar Bandari received his Ph.D. degree from, NIT Warangal, India in 2018. Received postdoctoral fellowship from GIGA Korea project at Seoul National University, South Korea, 2018-2019. Received ERASMUS-MUNDUS Euphrates scholarship from the European Union under the doctoral mobility programme at TEI of Patras, Greece (now changed to University of the Peloponnese), 2014-2015. He is twice scholarship holder from MHRD India. Since 2019, he has been with the NIT Meghalaya, India, as an Assistant Professor of Electronics and Communication Engineering. His research interests include future wireless systems, multi-carrier waveforms for next-generation wireless systems, multi-antenna/multi-user channels, compressed sensing, and cognitive radio.



V. Venkata Mani received the B.E. and M.E. degrees in electronics and communication engineering from the College of Engineering, Andhra University, India, in 1992 and 2003, respectively, and the Ph.D. degree in electrical engineering from the IIT Delhi, India, in 2009. She joined the Electronics and Communication Engineering Department, at NIT Warangal, in April 2008, as an Assistant Professor, where she has been a Professor, since July 2022. She has numerous publications in credit in national and international conferences and journals. Her research interests include wireless communication and signal processing for communication. She is a fellow of the IETE, India.



Anastasios Drosopoulos received his BSc (Physics) from the University of Patras, Greece, and the PhD (Electrical Engineering), from McMaster, Canada. From 1991 to 1997, he worked at the Defense Research Establishment, Ottawa, Canada, on Synthetic Aperture Radar Applications. From 1997 to 1999 he was with Nortel, Ottawa, Canada, in the area of optical communications. From 1999 to 2003 he was with Atmel Multimedia and Communications, Patras, Greece branch, in wireless communications. In 2003 he joined the Electrical Engineering Department of TEI of Western Greece (prior TEI of Patras) as a professor. With the amalgamation of TEI with the University of Peloponnese (2019) this became the Department of Electrical and Computer Engineering. His current interests include applications and modelling of electrical energy and communication systems.